



Cite this: *Nanoscale*, 2024, **16**, 1304

## Electrochemical impedance spectroscopy, another arrow in the arsenal to study the biodegradability of two-dimensional materials†

Livia Didonè, <sup>a</sup> Yunseok Shin, <sup>b</sup> Alessandro Silvestri, <sup>\*†c</sup> Maurizio Prato, <sup>c,d,e</sup> Sungjin Park <sup>\*b</sup> and Alberto Bianco <sup>\*a</sup>

Carbon nitride (C<sub>3</sub>N<sub>4</sub>) is an innovative material with a high potential in many applications including energy storage, catalysis, composites, and biomedicine. C<sub>3</sub>N<sub>4</sub> appears remarkably interesting not only for its properties but also because its simple preparation routes involve low-cost starting materials and reagents. However, there is still a lack of information on its degradability. For this reason, in this study, we evaluate the environmental persistence of C<sub>3</sub>N<sub>4</sub> and its oxidized form by applying the photo-Fenton reaction. The morphological and structural changes of both materials were monitored by transmission electron microscopy and Raman spectroscopy respectively. In addition, electrochemical impedance spectroscopy has been used as an original technique to validate the degradation process of C<sub>3</sub>N<sub>4</sub>.

Received 7th September 2023,  
Accepted 14th December 2023

DOI: 10.1039/d3nr04502a

rsc.li/nanoscale

### Introduction

Graphitic carbon nitride (C<sub>3</sub>N<sub>4</sub>), characterized by a triazine or a tris-triazine pattern, is a two-dimensional (2D) material that can be produced from three-dimensional (3D) C<sub>3</sub>N<sub>4</sub> *via* exfoliation. C<sub>3</sub>N<sub>4</sub> contains C and N atoms arranged in hexagonal rings made of C=N bonds with sp<sup>2</sup> hybridization, resulting in a π-conjugated framework.<sup>1</sup> This class of materials is receiving a lot of interest, not only for its remarkable properties but also because its preparation route involves low-cost starting materials and reagents.<sup>2</sup> In fact, abundant and inexpensive precursors, such as cyanamide, dicyanamide, or urea, can be used. The synthesis of C<sub>3</sub>N<sub>4</sub> is performed using a pyrolytic process, consisting of the decomposition of the carbon and

nitrogen sources, to produce volatile substances and solid residues.

Graphitic carbon nitrides have drawn a lot of attention due to their features, which can be attributed to their layered structure. Besides the simplicity of its synthesis, this material is characterized by high stability, low toxicity, wide visible light absorption range, and an ideal semiconducting behavior. Different C<sub>3</sub>N<sub>4</sub> are currently applied for photocatalysis and energy storage.<sup>3,4</sup> For example, they are used as anodic components in rechargeable lithium-ion batteries.<sup>5</sup> Moreover, C<sub>3</sub>N<sub>4</sub> can be used as saturable absorber,<sup>6</sup> or in membranes, in solar and fuel cells, and they are effective in removing contaminants from water, air, and soil.<sup>7,8</sup> Since C<sub>3</sub>N<sub>4</sub> resulted to be biocompatible, its use in biomedicine, biosensors, for photocatalytic sterilization, photodynamic therapy, and as drug carriers has been exploited.<sup>9</sup> Recently, C<sub>3</sub>N<sub>4</sub> was evaluated as an efficient carrier for the anticancer drug cisplatin.<sup>10</sup> Nevertheless, it must always be considered that the interaction of nanoparticles with the biological systems or the environment might generate toxic effects due to their small size, large surface area, and high reactivity. Overall, the physicochemical properties of a nanomaterial have a huge influence on its safety. For example, the degree of dispersion of carbon nanomaterials has an impact on their *in vitro* and *in vivo* toxicity.<sup>11</sup> In order to broaden C<sub>3</sub>N<sub>4</sub> applications in the biomedical and other fields, it is fundamental to examine the degradability profiles of this 2D material. The reported cytotoxicity effects of C<sub>3</sub>N<sub>4</sub> and other carbon-based nanomaterials include reactive oxygen species generation, DNA damage, lysosomal damage, mitochondrial dysfunction, and eventual cell death *via* necro-

<sup>a</sup>CNRS, UPR3572, Immunology, Immunopathology and Therapeutic Chemistry, ISIS, University of Strasbourg, 67000 Strasbourg, France.

E-mail: a.bianco@ibmc-cnrs.unistra.fr

<sup>b</sup>Department of Chemistry and Chemical Engineering, Inha University, 100 Inha-ro, Nam-gu, Incheon 22212, Korea. E-mail: sungjinpark@inha.ac.kr

<sup>c</sup>Center for Cooperative Research in Biomaterials (CIC biomAGUNE), Basque Research and Technology Alliance (BRTA), Paseo de Miramón 194, 20014 Donostia, San Sebastián, Spain

<sup>d</sup>Ikerbasque, Basque Foundation for Science, 48013 Bilbao, Spain

<sup>e</sup>Dipartimento di Scienze Chimiche e Farmaceutiche, INSTM UdR Trieste, University of Trieste Via Licio Giorgieri 1, 34127 Trieste, Italy

† Electronic supplementary information (ESI) available. See DOI: <https://doi.org/10.1039/d3nr04502a>

‡ Current address: Department of Molecular Sciences and Nanosystems, Ca' Foscari University of Venice, 30170, Venice, Italy. E-mail: alessandro.silvestri@unive.it

sis or apoptosis.<sup>12,13</sup> Cellular assays on lung epithelial cell lines (e.g., A549) showed that for  $C_3N_4$  the toxicity resulted to be dose-dependent, and it was generally rated lower than other 2D materials, such as graphene oxide (GO).<sup>14</sup>

However, no data is available on the (bio)degradability of  $C_3N_4$ . Thus, it is crucial to assess the degradability of this type of carbon-based nanomaterials, to foresee and limit their impact on health and the environment. A substance can undergo a mechanical, chemical, or biological degradation process. Biodegradation aims to bio-transform, recycle, and detoxify the concerned material. For example, in the biomedical field, it is crucial to consider the degradation of a therapeutic nanomaterial, since it should occur at the most proper time and place, namely the targeted pathological site, to allow the pharmacological benefit to take place.<sup>15</sup> Through the years, many studies on carbon-based nanomaterial degradation have been reported, but there is a lack of information regarding the degradability of  $C_3N_4$ . Overall, it was demonstrated that carbon-based nanomaterials are sensitive to the treatment with different types of peroxidases, where hydrogen peroxide is involved in the catalytic process. For example, it was shown that the biodegradation of GO by human myeloperoxidase is dispersibility-dependent.<sup>16</sup> Moreover, it was proven that the degradation of GO performed by horseradish peroxidase (HRP) is accelerated and more efficient when GO is functionalized with coumarin or catechol, which are specific ligands of HRP.<sup>17</sup> In this regard, the concept of degradation-by-design has been proposed, where the chemical functionalization of 2D materials enhances their degradability, and, accordingly, their safety.<sup>18</sup> In another study, graphene quantum dots (GQDs) were degraded by myeloperoxidase (MPO) *via* an oxidative enzymatic process.<sup>19</sup>

Many of the studies focused on the biodegradation of carbon-based nanomaterials are based on the simulation of oxidative conditions, in order to evaluate the behavior of a particular material when it comes in contact with the environment or a living organism. According to the literature, oxidative enzymes such as HRP and MPO are efficient agents for the biodegradation of carbon-based nanomaterials.<sup>20</sup> In addition to enzyme-catalyzed biodegradation, in an environmental context, the photo-Fenton reaction showed also significant results<sup>21</sup> and has been widely used to decompose aromatic organic pollutants in water.<sup>22</sup>

Since there is no sufficient knowledge regarding the degradation of graphitic carbon nitrides, we relied on our previous study conducted on the biodegradation of hexagonal boron nitride (hBN), since this material is known for its chemical inertness and high oxidation resistance.<sup>23</sup> The photo-Fenton reaction was applied as a first approach to study  $C_3N_4$  degradation in environmental conditions. This model reaction was chosen to develop effective tools to monitor the  $C_3N_4$  degradation process, that in future works will be applied to the enzymatic degradation. The photo-Fenton reaction is a UV-assisted version of the Fenton reaction, where the UV light enhances the degradation rate, by accelerating the production of chemically reactive hydroxyl radicals.

The effects of this reaction were monitored by transmission electron microscopy (TEM) imaging and by electrical impedance spectroscopy (EIS). EIS is a novel technique in the study of 2D material degradation, based on the perturbation of an electrochemical system in the equilibrium state, through the application of an oscillating voltage over a wide range of frequencies. The sinusoidal current response is monitored and the resistance of the material is recorded as a function of the perturbation frequency (impedance). EIS is a powerful technique able to discriminate, in the frequency domain, the electrochemical events occurring contemporarily at the interface between the material and the electrolyte. Therefore, EIS is a unique tool to investigate the changes in the material properties in relation to the surface structure and chemical composition. Based on these principles, EIS is largely used in the study of metal corrosion. Although 2D material degradation is conceptually a similar event, EIS has never been applied in this field.

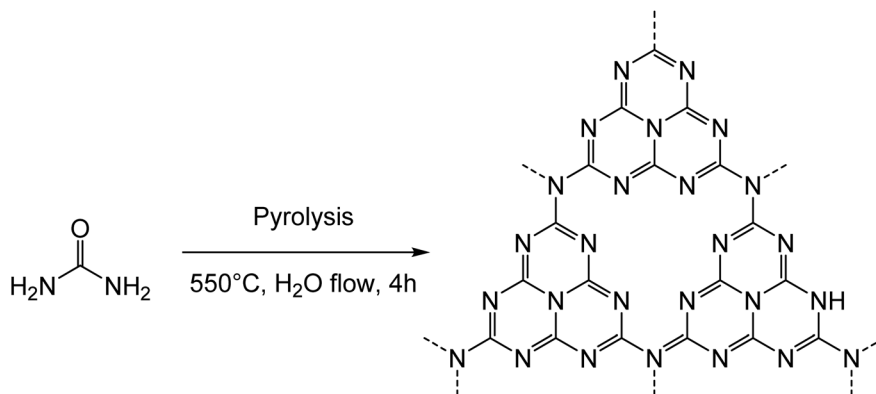
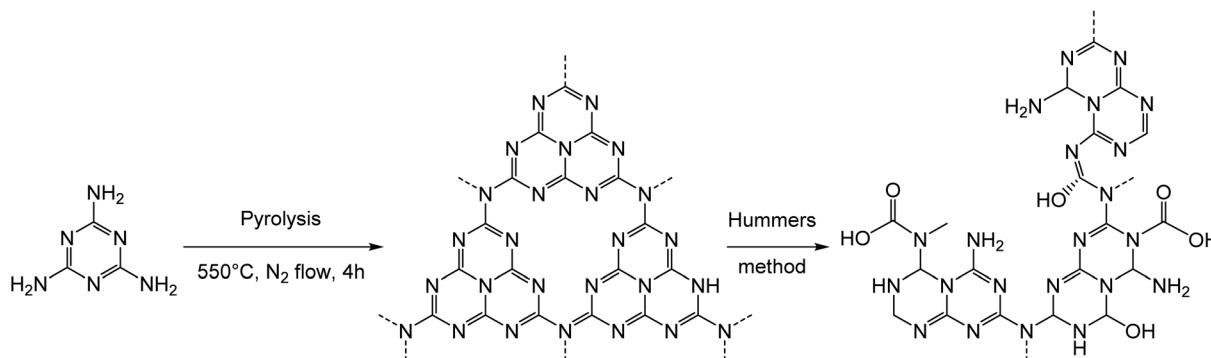
## Results and discussion

In this work, the photo-Fenton reaction was used to assess the biodegradability of two different samples of  $C_3N_4$ , corresponding to a material obtained from pyrolysis of urea (termed  $CN_{Urea}$ , CN standing for carbon nitride) and to a material prepared from pyrolysis of melamine followed by the Hummers' treatment to obtain a material rich on oxygenated functions (termed  $oxCN_{Mel}$ ).  $CN_{Urea}$  was obtained as a pale-yellow powder by thermal polycondensation of urea at 550 °C under a flow of air/ $H_2O$  gas (Scheme 1).<sup>24</sup>

The second sample ( $oxCN_{Mel}$ ) was synthesized by a two-step process starting from melamine. Heat treatment of melamine generated carbon nitride materials, followed by a chemical modification using  $H_2SO_4$  and  $KMnO_4$  as strong oxidizing reagents, afforded  $oxCN_{Mel}$  (Scheme 2). The purpose was to obtain a material that would be easier to degrade, owing to the presence of the oxygenated functions. We point out that it was not possible to obtain this oxidized form of carbon nitride from  $CN_{Urea}$  because this latter is too sensitive to strong acidic conditions, which lead to complete degradation during the oxidation process. This can be considered a novel route to produce small sheets of water-dispersible and atomically thin oxidized carbon nitride-based materials.<sup>25</sup>

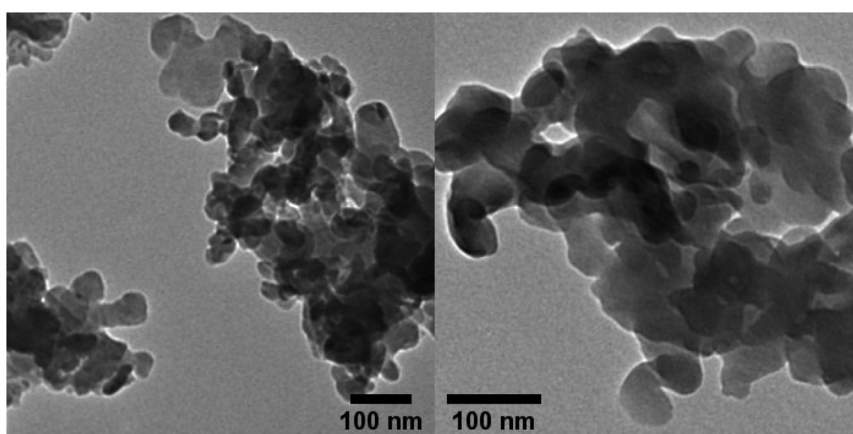
Both  $CN_{Urea}$  and  $oxCN_{Mel}$  were characterized using complementary spectroscopic and microscopic techniques (see data and discussion in ESI, Fig. S1–S7†). The characterization revealed that  $CN_{Urea}$  contains tri-*s*-triazine-based crystalline  $C_3N_4$  structures, while  $oxCN_{Mel}$  contains heavily oxidized  $C_3N_4$ -based structures with significantly damaged  $sp^2$  networks.

For the degradability studies, stock water dispersions ( $0.78 \text{ mg mL}^{-1}$ ) were prepared using a cup-horn sonicator, operating for 60 min. The photo-Fenton reaction was then applied by incubating the dispersions of the two materials in an acidic aqueous solution, where  $FeCl_3$  and  $H_2O_2$  were regularly added as catalysts. In acidic conditions,  $Fe^{3+}$  mainly exists

Scheme 1 Synthesis of CN<sub>Urea</sub>.Scheme 2 Synthesis and proposed structure of oxCN<sub>Mel</sub>.

as Fe(OH)<sup>2+</sup>, and effectively absorbs UV light. In this way, a disproportionation occurs being Fe(OH)<sup>2+</sup> transformed into Fe<sup>2+</sup> and hydroxyl radicals, that generate the oxidation conditions of the materials (Fig. S8†). The process is accelerated by UV irradiation at a wavelength of 365 nm. The reaction to degrade both carbon nitride materials was carried out for 100 h at room temperature, by renewing FeCl<sub>3</sub> every 35 h and H<sub>2</sub>O<sub>2</sub>

every 10 h. TEM is commonly employed to follow the progress of the nanomaterial degradation,<sup>20</sup> even though this technique provides qualitative rather than quantitative results. Before starting the degradation process, CN<sub>Urea</sub> appears round shaped and organized as layered structures. Despite the long sonication process, the particles are not homogeneously distributed on the grid, but they are present as aggregates (Fig. 1).

Fig. 1 TEM images of CN<sub>Urea</sub> dispersed in water.

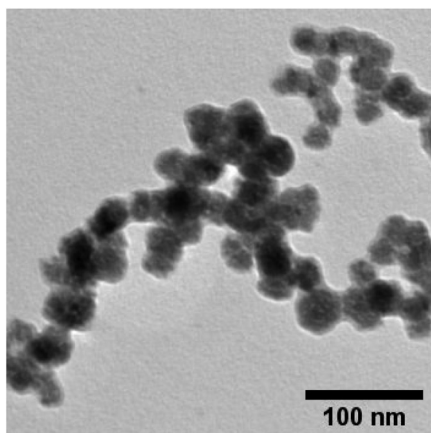


Fig. 2 TEM images of  $\text{CN}_{\text{Urea}}$  after 50 h treatment.

TEM images of the samples were captured at different time points. To monitor the process of degradation on the material, and to obtain significant information about the morphological

changes, the samples were observed first after 50 h (Fig. 2). At this time point, some pores inside the structure started forming, but it is after 100 h that the edges appear jagged and the number of holes in the material becomes more significant (Fig. 3).

We already proved that the treatment of hBN for 100 h in the conditions of the photo-Fenton reaction resulted in the successful degradation of the material, since its 2D layered structure was completely lost at the end of the process. During this experiment with  $\text{C}_3\text{N}_4$ , we expected to achieve a similar result in the same time frame. However, even if the TEM images allow us to state that the oxidation process has modified the material, the degradation was not completed.

The TEM analysis of  $\text{oxCN}_{\text{MeI}}$  before degradation, evidenced a less homogeneous material, with many irregular layers surrounding one another (Fig. 4).

To evaluate the degradation of  $\text{oxCN}_{\text{MeI}}$ , the samples were observed again after 50 and 100 h of reaction. In the middle of the process, no significant changes were visible (Fig. 5, left). However, at the end of the photo-Fenton reaction, the morphology of the material showed evident modifications (Fig. 5,

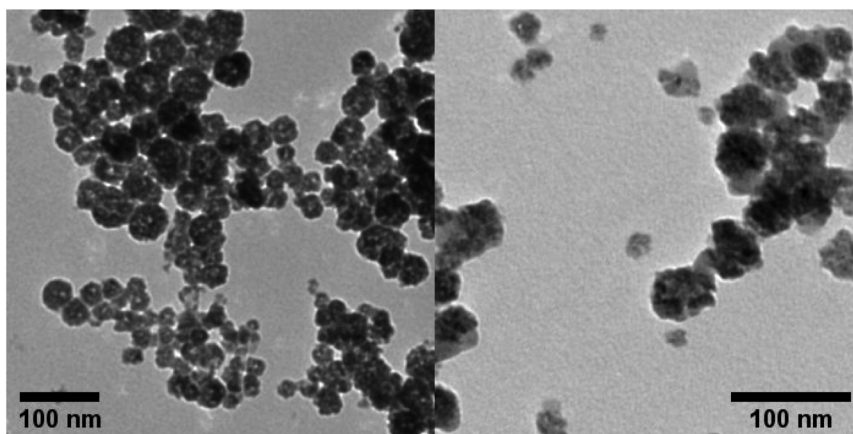


Fig. 3 TEM images of  $\text{CN}_{\text{Urea}}$  after 100 h treatment.

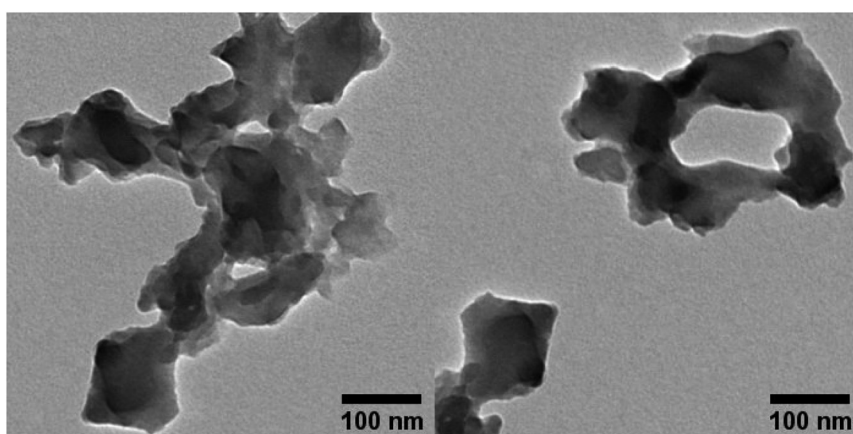


Fig. 4 TEM images of  $\text{oxCN}_{\text{MeI}}$  dispersed in water.



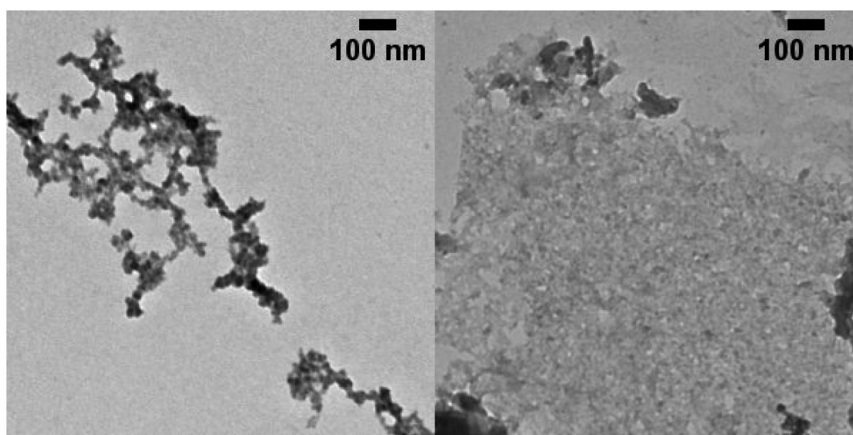


Fig. 5 TEM images of oxCN<sub>Mel</sub> after 50 (left) and 100 h (right) treatment.

right). In fact, there are holes inside the structure, and the edges appear fragmented.

Overall, for both materials, the results of the TEM analysis show an incomplete degradation of the starting material by the end of the experiments. This suggests that the degradation took place, but only partially. Moreover, inspired by the study of hBN degradation,<sup>23</sup> Raman spectroscopy was considered as an additional characterization technique to follow the degradation process. This kind of spectroscopy is known to be remarkable not only for being nondestructive, fast and high-resolution, but also for its ability to provide a comprehensive overview of the structural electronic information of a material.<sup>26</sup> Carbon-based nanomaterials present diagnostic bands in the Raman spectrum that correspond directly to a specific vibrational frequency of a molecular bond. During the degradation process, it is likely to observe the decrease in intensity of these distinguishing peaks. For example, a complete disappearance of the band was seen at the end of the photo-Fenton degradation of hBN.<sup>23</sup> In the case of C<sub>3</sub>N<sub>4</sub> both in powder and on the residue obtained depositing and drying the solution on a silica wafer, CN<sub>Urea</sub> and oxCN<sub>Mel</sub> revealed a very strong autofluorescence, which hampered the observation and evolution of their characterizing peaks during the photo-Fenton process (Fig. S9†).

Although TEM allowed to see the onset of the biodegradation process of these two types of carbon nitrides, the need to broaden the understanding of this phenomenon was relevant. To this aim, EIS proved to be effective. EIS is an electrochemical technique used to study the phenomena happening at the interface of an electrode and a solution of electrolyte. When an electrode is immersed in an electrolyte and polarized, a series of phenomena take place at the liquid–solid interface. Some of the main phenomena involved include the formation of an electrical double layer at the interface, charge transfer through the materials, and the diffusion of chemical species from the bulk of the electrolyte to the surface.<sup>27</sup> Although all these phenomena take place at the same time, EIS can resolve them by applying an oscillating potential to the

electrode and measuring the impedance in function of the frequency. The contribution of each of these processes depends on the chemical composition of the material at the interface and on its morphology.<sup>28</sup> The photo-Fenton reaction is expected to degrade C<sub>3</sub>N<sub>4</sub> modifying its morphology, oxidation degree and introducing defects in the crystalline structure affecting the behavior of the material at the interface with an electrolyte solution. To confirm our hypothesis and prove that EIS can be used to study the degradation of 2D materials, we drop-cast aliquots of the two types of C<sub>3</sub>N<sub>4</sub> on top of a glassy carbon electrode (GCE), sampled at time 0 and 100 h of the photo-Fenton reaction. Potassium ferricyanide (K<sub>3</sub>[Fe(CN)<sub>6</sub>]) was used as an electrochemical mediator to investigate the phenomena happening at the interface with the material.  $E_{1/2}$  of K<sub>3</sub>[Fe(CN)<sub>6</sub>] (0.21 V) was selected as operational potential, as at this potential the mediator generates a faradaic current, which is exploited to study the properties of the material. Small perturbations of 10 mV were applied with a range of frequencies between 100 kHz and 10 mHz. In Fig. 6A and C it is possible to see the Bode plots for CN<sub>Urea</sub> and oxCN<sub>Mel</sub>, representing the impedance of the material in function of applied frequency. At high frequencies (up to 1 kHz) the value of impedance is constant and does correspond to the uncompensated resistance of the electrochemical system. In the middle region, we can see an increase in the impedance due to the charge transfer process across the material. Finally, the rapid increase in the impedance at low frequencies can be attributed to the formation of a depletion layer, due to the consumption of the mediator close to the electrode surface. When this happens, the value of impedance is governed by the diffusion rate of the electrochemical mediator from the bulk of the solution to the surface of the electrode.<sup>28</sup>

In case of both CN<sub>Urea</sub> and oxCN<sub>Mel</sub>, higher values of impedance were recorded for the samples which underwent the photo-Fenton reaction. However, for oxCN<sub>Mel</sub> the difference is less pronounced, as the starting material was already oxidized and presented a higher impedance compared to CN<sub>Urea</sub>. The Nyquist plots (Fig. 6B and D) represent the imaginary ( $Z''$ ) part

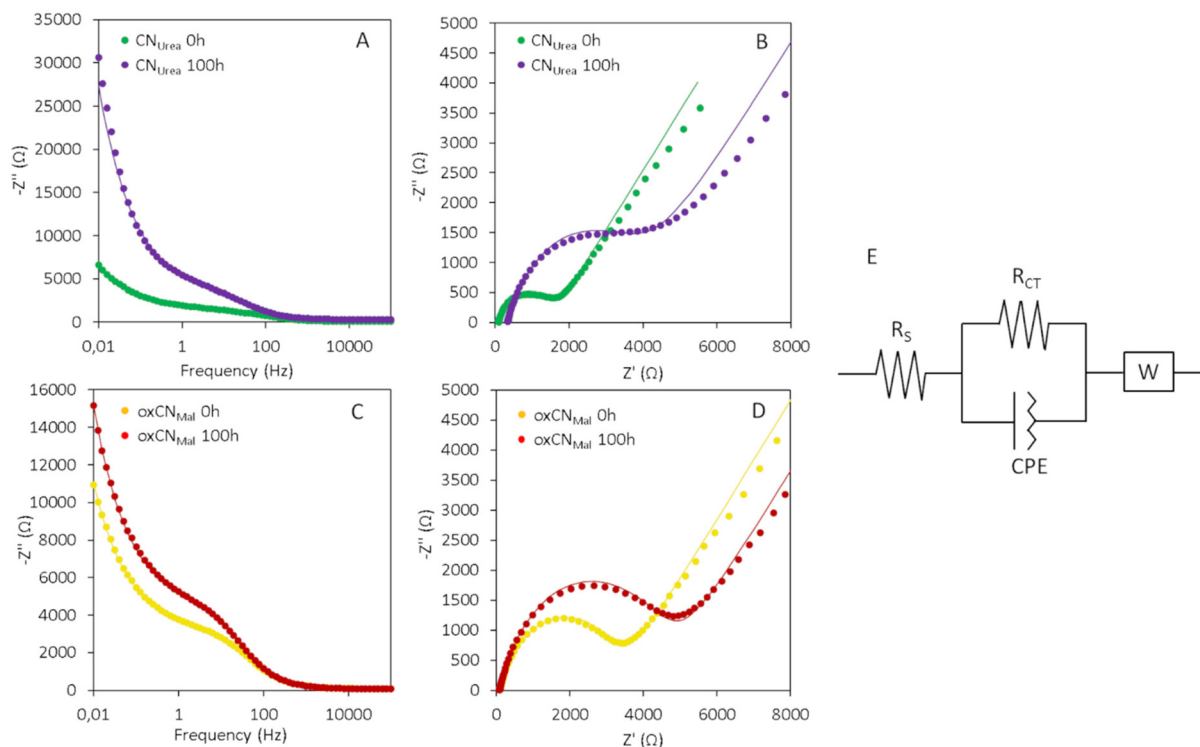


**Fig. 6** EIS measurements were obtained by drop casting  $1 \text{ mg ml}^{-1}$  of  $\text{C}_3\text{N}_4$  on a GCE electrode, in a solution of  $5 \text{ mM}$  of  $\text{K}_3[\text{Fe}(\text{CN})_6]$ . A potential of  $0.21 \text{ V}$  (vs. reference) was applied with a perturbation of  $10 \text{ mV}$  in a range of frequencies between  $100 \text{ kHz}$  and  $10 \text{ mHz}$ . (A) Bode plot of  $\text{CN}_{\text{Urea}}$  before ( $0 \text{ h}$ ) and after ( $100 \text{ h}$ ) the photo-Fenton reaction. The dots represent the experimental data, and the line is the fitting. (B) Nyquist plot of  $\text{CN}_{\text{Urea}}$  before ( $0 \text{ h}$ ) and after ( $100 \text{ h}$ ) the photo-Fenton reaction. (C) Bode plot of  $\text{oxCN}_{\text{Mel}}$  before ( $0 \text{ h}$ ) and after ( $100 \text{ h}$ ) the photo-Fenton reaction. (D) Nyquist plot of  $\text{oxCN}_{\text{Mel}}$  before ( $0 \text{ h}$ ) and after ( $100 \text{ h}$ ) the photo-Fenton reaction. (E) Scheme of the equivalent circuit used to fit the EIS data.

of the impedance plotted as a function of the real one ( $Z'$ ). These graphs give a good visual interpretation of the phenomena taking place at the interface of the electrode. The semi-circle at the beginning of the curve confirms the presence of a charge transfer process. The larger is the diameter of the semi-circle, the higher is the resistance of the material at the electron transfer. The tail of the curve with a slope of  $45^\circ$  is representative of the diffusion processes taking place from the bulk of the solution to the interface. From the Nyquist plot, it is possible to extrapolate quantitative data, by fitting it with an equivalent circuit. The circuit chosen in this work is represented in Fig. 6E and is composed of a parallel resistance and a constant phase element (CPE) in series with a Warburg (W) element.  $R_s$  represents the uncompensated resistance.  $R_{\text{CT}}$  represents the resistance to electron transfer imposed by  $\text{C}_3\text{N}_4$ . CPE is an imperfect capacitor and represents the formation of a double layer of charges at the interface with the electrolyte. Finally, W is a mathematical equation representing the diffusive process. The most significant value that can be obtained from the fitting is the  $R_{\text{CT}}$ . For  $\text{CN}_{\text{Urea}}$ ,  $R_{\text{CT}}$  increases drastically after the photo-Fenton process from  $1.38 \text{ k}\Omega$  to  $3.06 \text{ k}\Omega$  indicating that the reaction induces the formation of defects and oxidized sites in the carbon nitride structure, and therefore can partially degrade it. Due to the Hummers oxi-

dative process, the charge transfer resistance of the  $\text{oxCN}_{\text{Mel}}$  is instead high already before the photo-Fenton reaction ( $3.1 \text{ k}\Omega$ ). Control reactions without Fe,  $\text{H}_2\text{O}_2$ , or UV light treatment were performed. In the three cases no variation of the resistance was detected, confirming that in the absence of one of the three factors the degradation does not take place (Fig. S10†). The evolution in time of the  $\text{C}_3\text{N}_4$  degradation process was investigated by taking aliquots from the reaction mixture at the time points  $20 \text{ h}$  and  $50 \text{ h}$  (Fig. S11†). Due to the reduced volume of the aliquots, less material was available to perform these time-resolved measurements. Consequently, we drop cast  $10 \mu\text{l}$  of  $0.1 \text{ mg ml}^{-1}$   $\text{C}_3\text{N}_4$  solution on the GCE. The lower amount of  $\text{C}_3\text{N}_4$  deposited resulted in higher charge transfer resistance values. Nevertheless, the trend seen in Fig. 6 is confirmed: the resistance to the charge transfer of both  $\text{CN}_{\text{Urea}}$  and  $\text{oxCN}_{\text{Mel}}$  increases with time, corroborating that this effect is correlated with progressive material degradation. Furthermore, these data confirm that the changes in  $R_{\text{CT}}$  for  $\text{oxCN}_{\text{Mel}}$  are less prominent, since the oxidized material presents higher charge resistance values before the photo-Fenton reaction.

In summary, the results of TEM and EIS evidenced a partial degradation of the two carbon nitrides during the course of the photo-Fenton reaction. While the onset of  $\text{CN}_{\text{Urea}}$  bio-

degradation was clearly demonstrated, the morphological changes in oxCN<sub>MeI</sub> were more difficult to assess. This is likely because the initial oxidation of this material already disrupted its graphitic structure, resulting in a difficult distinction of the contribution of the Hummers reaction from the oxidative degradation operated by the photo-Fenton reaction. In conclusion, the synergy between the two spectroscopic and microscopic methods used in this study contributed to a better understanding the degradation process of graphitic carbon nitrides and could be applied to other 2D materials.

## Author contributions

A. B., A. S. and S. P. planned the experiments. L. D., Y. S. and A. S. carried out the experiments. L. D., Y. S., A. S. and A. B. analyzed the data. A. B., S. P. and M. P. searched for funding. L. D., Y. S., A. S., S. P. and A. B. wrote the manuscript. All authors read and commented the manuscript.

## Conflicts of interest

There are no conflicts to declare.

## Acknowledgements

We gratefully acknowledge the financial support from PHC STAR Program 2022 (Project 47404TA), Centre National de la Recherche Scientifique (CNRS), Jean-Marie Lehn Foundation, and Interdisciplinary Thematic Institute SysChem *via* the IdEx Unistra (ANR-10-IDEX-0002) within the program Investissement d'Avenir. The authors are indebted to Cathy Royer from the Plateforme Imagerie *In Vitro* de l'ITI Neurostra for SEM analyses. S. Park and Y. Shin were supported by National Research Foundation of Korea (NRF) grants funded by the Korean government (MSIT) (NRF-2021R1A2B5B02001587 and 2021K1A3A1A21039034). L. D. wish to thank the Erasmus+ Program from the University of Trieste (Italy). We also thank L. Jacquemin, R. Soltani, Y. He and I. Janica for their help on XPS and Raman analyses.

## References

- N. Baig, *Composites, Part A*, 2023, **165**, 107362.
- T. K. Mukhopadhyay, L. Leherter and A. Datta, *J. Phys. Chem. Lett.*, 2021, **12**, 1396–1406.
- C. Rosso, G. Filippini, A. Criado, M. Melchionna, P. Fornasiero and M. Prato, *ACS Nano*, 2021, **15**, 3621–3630.
- G. Filippini, F. Longobardo, L. Forster, A. Criado, G. Di Carmine, L. Nasi, C. D'Agostino, M. Melchionna, P. Fornasiero and M. Prato, *Sci. Adv.*, 2020, **6**, eabc9923.
- T. S. Miller, A. B. Jorge, A. Sella, F. Corà, P. R. Shearing, D. J. L. Brett and P. F. McMillan, *Electroanalysis*, 2015, **27**, 2614–2619.
- M. Wang, F. Ma, Z. Wang, D. Hu, X. Xu and X. Hao, *Photonics Res.*, 2018, **6**, 307.
- D. Jang, S. Lee, N. H. Kwon, T. Kim, S. Park, K. Y. Jang, E. Yoon, S. Choi, J. Han, T. W. Lee, J. Kim, S. J. Hwang and S. Park, *Carbon*, 2023, **208**, 290–302.
- D. Jang, S. Park, S. Choi, J. Kim and S. Park, *J. Photochem. Photobiol., A*, 2023, **443**, 114840.
- S. Che, L. Zhang, T. Wang, D. Su and C. Wang, *Adv. Sustainable Syst.*, 2022, **6**, 2100477.
- M. Perveen, S. Nazir, A. W. Arshad, M. I. Khan, M. Shamim, K. Ayub, M. A. Khan and J. Iqbal, *Biophys. Chem.*, 2020, **267**, 106461.
- X. Yuan, X. Zhang, L. Sun, Y. Wei and X. Wei, *Part. Fibre Toxicol.*, 2019, **16**, 18.
- H. Taheri, M. A. Unal, M. Sevim, C. Gurcan, O. Ekim, A. Ceylan, Z. Syrgiannis, K. C. Christoforidis, S. Bosi, O. Ozgenç, M. J. Gómez, M. Turktas Erken, Ç. Soydal, Z. Eroğlu, C. V. Bitirim, U. Cagin, F. Arı, A. Ozen, O. Kuçuk, L. G. Delogu, M. Prato, Ö. Metin and A. Yilmazer, *Small*, 2020, **19**, 1904619.
- B. Fadeel, C. Bussy, S. Merino, E. Vázquez, E. Flahaut, F. Mouchet, L. Evariste, L. Gauthier, A. J. Koivisto, U. Vogel, C. Martín, L. G. Delogu, T. Buerki-Thurnherr, P. Wick, D. Beloin-Saint-Pierre, R. Hischer, M. Pelin, F. Candotto Carniel, M. Tretiach, F. Cesca, F. Benfenati, D. Scaini, L. Ballerini, K. Kostarelos, M. Prato and A. Bianco, *ACS Nano*, 2018, **12**, 10582–10620.
- Q. Dong, N. M. Latiff, V. Mazánek, N. F. Rosli, H. L. Chia, Z. Sofer and M. Pumera, *ACS Appl. Nano Mater.*, 2018, **1**, 4442–4449.
- R. R. Remya, A. Julius, T. Y. Suman, V. Mohanavel, A. Karthick, C. Pazhanimuthu, A. V. Samrot and M. Muhibbullah, *J. Nanomater.*, 2022, **2022**, 6090846.
- R. Kurapati, J. Russier, M. A. Squillaci, E. Treossi, C. Ménard-Moyon, A. E. Del Rio-Castillo, E. Vazquez, P. Samorì, V. Palermo and A. Bianco, *Small*, 2015, **11**, 3985–3994.
- R. Kurapati, F. Bonachera, J. Russier, A. R. Sureshbabu, C. Ménard-Moyon, K. Kostarelos and A. Bianco, *2D Mater.*, 2018, **5**, 015020.
- A. R. Sureshbabu, R. Kurapati, J. Russier, C. Ménard-Moyon, I. Bartolini, M. Meneghetti, K. Kostarelos and A. Bianco, *Biomaterials*, 2015, **72**, 20–28.
- C. Martín, G. Jun, R. Schurhammer, G. Reina, P. Chen, A. Bianco and C. Ménard-Moyon, *Small*, 2019, **15**, 1905405.
- B. Ma, C. Martín, R. Kurapati and A. Bianco, *Chem. Soc. Rev.*, 2020, **49**, 6224–6247.
- X. Luan, C. Martín, P. Zhang, Q. Li, I. A. Vacchi, L. G. Delogu, Y. Mai and A. Bianco, *Angew. Chem., Int. Ed.*, 2020, **59**, 18515–18521.
- X. Zhou, Y. Zhang, C. Wang, X. Wu, Y. Yang, B. Zheng, H. Wu, S. Guo and J. Zhang, *ACS Nano*, 2012, **6**, 6592–6599.
- R. Kurapati, C. Backes, C. Ménard-Moyon, J. N. Coleman and A. Bianco, *Angew. Chem., Int. Ed.*, 2016, **55**, 5506–5511.

- 24 D. Jang, S. Choi, N. H. Kwon, K. Y. Jang, S. Lee, T. W. Lee, S. J. Hwang, H. Kim, J. Kim and S. Park, *Appl. Catal., B*, 2022, **310**, 121313.
- 25 J. Oh, R. J. Yoo, S. Y. Kim, Y. J. Lee, D. W. Kim and S. Park, *Chem. – Eur. J.*, 2015, **21**, 6241–6246.
- 26 A. C. Ferrari, *Solid State Commun.*, 2007, **143**, 47–57.
- 27 E. Barsoukov and J. R. Macdonald, *Impedance Spectroscopy: Theory, Experiment, and Applications*, John Wiley & Sons, Inc., 2018.
- 28 W. Hu, Y. Peng, Y. Wei and Y. Yang, *J. Phys. Chem. C*, 2023, **127**, 4465–4495.